Leishmania profilin interacts with actin through an unusual structural mechanism to control cytoskeletal dynamics in parasites

Andrea Vizcaíno-Castillo[1,‡], Tommi Kotila[1,‡], Konstantin Kogan[1,‡], Ryuji Yanase[2,‡], Juna Como[3], Lina Antenucci[1], Alphee Michelot[3], Jack D. Sunter[2,*], and Pekka Lappalainen[1,4,*]

From the [1]HiLIFE Institute of Biotechnology, University of Helsinki, Helsinki, Finland; [2]Oxford Brookes University, Department of Biological and Medical Sciences, Oxford, UK; [3]Aix Marseille University, CNRS, IBDM, Turing Centre for Living Systems, Marseille, France; [4]Faculty of Biological and Environmental Sciences, University of Helsinki, Helsinki, Finland

Reviewed by members of the JBC Editorial Board. Edited by Enrique De La Cruz

Diseases caused by *Leishmania* and *Trypanosoma* parasites are a major health problem in tropical countries. Because of their complex life cycle involving both vertebrate and insect hosts, and >1 billion years of evolutionary distance, the cell biology of trypanosomatid parasites exhibits pronounced differences to animal cells. For example, the actin cytoskeleton of trypanosomatids is divergent when compared with other eukaryotes. To understand how actin dynamics are regulated in trypanosomatid parasites, we focused on a central actin-binding protein profilin. Co-crystal structure of *Leishmania major* actin in complex with *L. major* profilin revealed that, although the overall folds of actin and profilin are conserved in eukaryotes, *Leishmania* profilin contains a unique α-helical insertion, which interacts with the target binding cleft of actin monomer. This insertion is conserved across the Trypanosomatidae family and is similar to the structure of WASP homology-2 (WH2) domain, a small actin-binding motif found in many other cytoskeletal regulators. The WH2-like motif contributes to actin monomer binding and enhances the actin nucleotide exchange activity of *Leishmania* profilin. Moreover, *Leishmania* profilin inhibited formin-catalyzed actin filament assembly in a mechanism that is dependent on the presence of the WH2-like motif. By generating profilin knockout and knockin *Leishmania mexicana* strains, we show that profilin is important for efficient endocytic sorting in parasites, and that the ability to bind actin monomers and proline-rich proteins, and the presence of a functional WH2-like motif, are important for the *in vivo* function of *Leishmania* profilin. Collectively, this study uncovers molecular principles by which profilin regulates actin dynamics in trypanosomatids.

The *Leishmania* parasites are the etiological agents of a group of diseases collectively known as leishmaniases. These parasites cause three main types of infections: cutaneous leishmaniasis, visceral leishmaniasis, also known as kala-azar, and mucocutaneous leishmaniasis. The severity of disease varies from asymptomatic to fatal if untreated. Despite a significant amount of research conducted on these parasites, leishmaniasis remains an important health problem with approximately 700,000 to 1,000,000 new cases per year (1, 2). The related *Trypanosoma* parasites also cause severe diseases, such as African sleeping sickness and Chagas disease. Both *Leishmania* and *Trypanosoma* genera belong to the Trypanosomatidae family of flagellated protozoan parasites (3).

Leishmania parasites have a complex life cycle that involves both insect vectors (sand flies) and mammalian hosts with differentiation into two major cell morphologies: flagellated motile promastigotes and macrophage-resident nonmotile amastigotes (4). Because of their unusual life cycle, and because the family of trypanosomatid parasites diverged early in the evolution from other eukaryotes (5), they exhibit biological peculiarities that deviate them from those of well-studied organisms, such as animals, yeasts, and plants. An interesting example of such biological features is their atypical cytoskeleton, which is considered to be mainly microtubule based (6). Also actin is present in trypanosomatid parasites, albeit its role seems to be limited to a subset of cellular processes (7–9). In animals, the actin cytoskeleton contributes to several cellular functions, including motility, morphogenesis, adhesion, vesicular traffic, cytokinesis, and endocytosis (10, 11), but according to current understanding, actin and actin-regulating proteins in trypanosomatids are mainly involved in endocytosis, vesicular trafficking, and assembly of flagellum, and hence important for the viability of these parasites (12–14). In *Leishmania*, actin may in addition be involved in kinetoplast remodeling during cell division (15).

Actin is an abundant protein, which is conserved throughout evolution from Asgard archaea to all eukaryotes (16). Globular actin monomers (G-actin) can spontaneously assemble into helical filaments (F-actin) in which actin subunits arrange in a head-to-tail orientation, creating two structurally distinct filament ends known as the barbed end and the pointed end. Furthermore, actin molecules bind an adenosine nucleotide, either ATP or ADP. Actin filament assembly occurs predominantly through incorporation of ATP–

---

‡ These authors contributed equally to this work.
* For correspondence: Pekka Lappalainen, pekka.lappalainen@helsinki.fi; Jack D. Sunter, jsunter@brookes.ac.uk.

actin monomers to the filament barbed end, and filament disassembly occurs mainly through dissociation of ADP–actin monomers from the filament pointed end. Filament turnover is powered by ATP, because in the filamentous form, actin catalyzes ATP hydrolysis, whereas ADP in an actin monomer can be exchanged for ATP to "recharge" the monomer for a new round of filament assembly. The coordinated actin filament polymerization produces pushing forces that, for example, promote formation of plasma membrane protrusions for cell migration and plasma membrane invaginations during endocytosis. In order to control actin filament assembly and disassembly in space and time, a large repertoire of actin-binding proteins (ABPs) evolved to regulate different aspects of actin dynamics. These include the Arp2/3 complex, which catalyzes nucleation of branched actin filament networks for endocytosis and cell migration, formins, which assemble linear actin filaments for other cellular processes, as well as a large array of proteins controlling actin filament disassembly and cytoplasmic actin monomer pool (11, 17).

Leishmania and *Trypanosoma* actins show ∼70% sequence identity to vertebrate actins, which makes them among the most divergent actins in the eukaryotic lineage (14). Despite the large divergence in sequence, recent structural and biochemical study on *Leishmania major* actin (LmActin) demonstrated that the conformation of actin filaments in *Leishmania* is nearly identical to their vertebrate counterparts. However, because of differences in the subunit–subunit interfaces, the parasite actin filaments display more rapid turnover compared with animal actin filaments. The same study also revealed that *L. major* cofilin fragments LmActin filaments more frequently compared with mammalian cofilin, demonstrating that both actin filaments and their interplay with cofilin display pronounced differences between animals and trypanosomatids (18).

Along with cofilin, a handful of other canonical ABPs are present in *Leishmania* and *Trypanosoma* species (14, 19). These include the small actin monomer–binding protein profilin, which is found in all eukaryotic organisms that contain a regulated actin cytoskeleton. In animals, yeasts, and plants, profilins inhibit spontaneous nucleation of actin filaments, promote elongation of pre-existing barbed ends of the actin filament, and prevent assembly of actin monomers to the filament pointed ends (11). Profilins can also accelerate the ADP-to-ATP nucleotide exchange on actin monomers (20–22). Besides binding actin, profilins also interact with polyproline-rich motifs, which are typical for actin filament nucleating/polymerizing proteins, such as formins (23). Formins are composed of formin homology 1 (FH1) and formin homology 2 (FH2) domains, which consists of polyproline stretches and interact with actin to promote filament assembly, respectively. Formins contain also other domains involved in regulation of their subcellular localization and activity (24). Interaction of profilin with the FH1 domain allows the delivery of actin monomer–profilin complexes to the adjacent FH2 domains. Hence, upon activation, formins typically work in synergy with profilin to accelerate actin filament assembly in cells (25–27). Profilin expression was also demonstrated in

trypanosomatids (28–30), but the mechanism by which this protein controls actin dynamics in *Leishmania* and *Trypanosoma* parasites has remained largely unclear. An earlier study reported that *Leishmania donovani* profilin binds polyproline peptides and accelerates nucleotide exchange on rabbit muscle actin. Moreover, depletion of profilin was reported to affect cellular growth and endocytic trafficking (30) and contribute to mitotic spindle orientation and cell cycle progression in *L. donovani* parasites (31). However, no structural information of trypanosomatid profilins is available, and all biochemical works so far have been performed by using a heterologous combination of mammalian and *Leishmania* actin and ABPs, which were recently demonstrated to be unfavorable substrates for each other (18). Thus, the mechanisms by which trypanosomatid profilins interact with actin monomers, and regulate actin dynamics together with other proteins, such as formins, have remained elusive.

To uncover how trypanosomatid profilins control actin dynamics, we determined the crystal structure of *L. major* profilin (LmProfilin) in complex with LmActin. Although the overall folds of actin and profilin are conserved in evolution, our structural work revealed that *Leishmania* profilin harbors a peculiar WASP homology-2 (WH2) domain–like α-helix, which makes contact with actin. Biochemical and genetic studies revealed that this insertion, which is conserved across the Trypanosomatidae family, is important for high-affinity actin monomer binding and nucleotide exchange *in vitro*, as well as for the proper function of profilin in endocytosis in *Leishmania* parasites. Moreover, we provide evidence that *Leishmania* profilin inhibits formin-catalyzed actin filament assembly through a mechanism that is dependent on the WH2 domain–like motif. These findings demonstrate that the actin monomer–profilin interplay is divergent in trypanosomatid parasites as compared with animals and propose that the specific structural features of actin–profilin interactions may serve as good targets for selectively neutralizing *Leishmania* and *Trypanosoma* parasites.

Results

Crystal structure of Leishmania *profilin–actin monomer complex*

To elucidate the mechanism by which trypanosomatid profilins interact with actin monomers to control cytoskeletal dynamics, we expressed and purified recombinant LmProfilin and LmActin and studied their interactions by X-ray crystallography. We obtained crystals of the *Leishmania* profilin in complex with an ATP–actin monomer and determined the structure of the complex at 2.2 Å resolution (Table S1). The structure revealed that *Leishmania* profilin forms a 1:1 stoichiometric complex with ATP–actin monomer and interacts with the barbed end face of the actin monomer at the border of actin subdomains 1 and 3, similar to other profilins (Fig. 1*A*). The overall fold of *Leishmania* profilin is also similar to the reported structures of profilins from other organisms, such as mammals, yeasts, malaria parasite, and Asgard archaea (21, 32–37). Furthermore, the conformation of *Leishmania* actin in
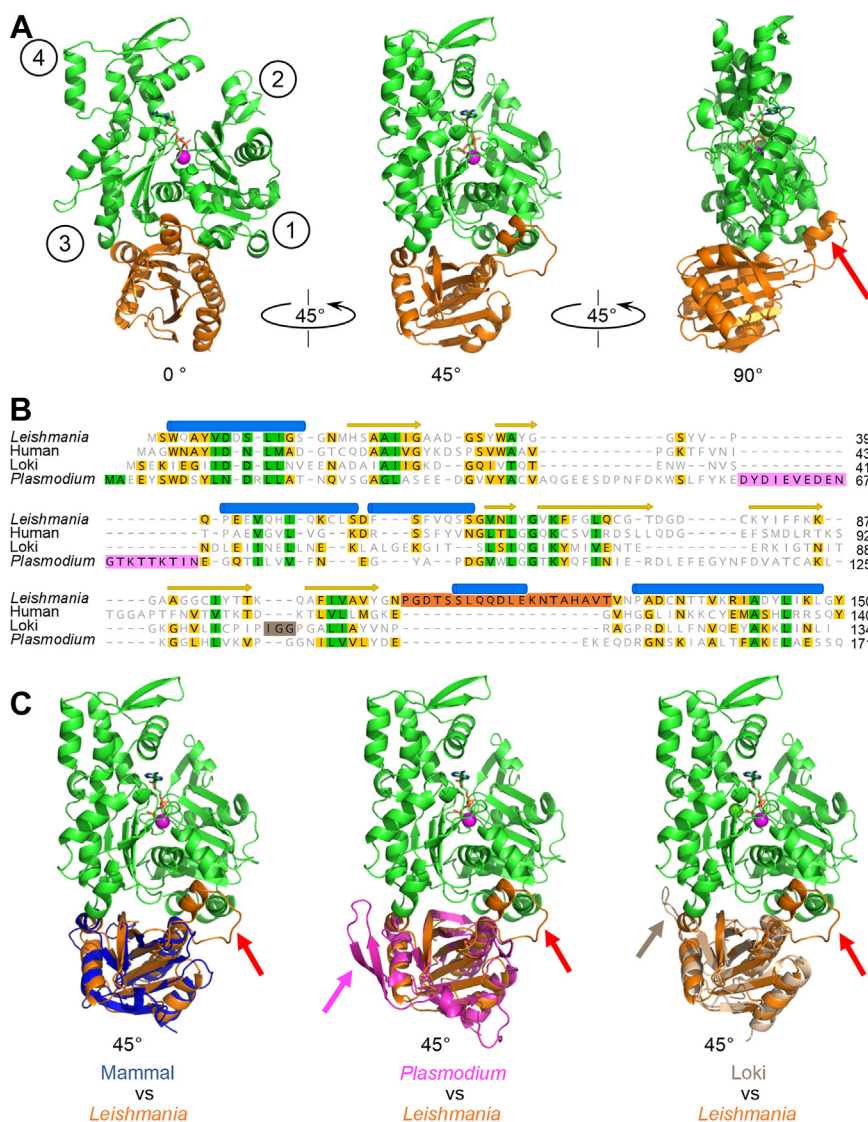
Figure 1. Crystal structure of *Leishmania major* profilin (LmProfilin) in complex with actin. *A*, three orientations (0°, 45°, and 90°) of the co-crystal structure of LmProfilin (*orange*)–actin (*green*) complex. The ATP nucleotide (*brown*) and the associated Ca^{2+} ion (*magenta* ball shaped) in actin are highlighted. The subdomains of actin are labeled by one to four numbers in *circles*. The specific insertion in *Leishmania* profilin is indicated with a *red arrow* in the panel on the *right*. *B*, structure-based protein sequence alignment (performed by Dali server (72)), of profilins from trypanosomatid parasite (*L. major*, Protein Data Bank [PDB] ID: 8C47, chain B; UniProt: Q4Q5N1), human (*Homo sapiens*, PDB ID: 6NBW, chain C; UniProt: P07737; (73)), Asgard archaea (Lokiarchaeum, PDB ID: 5ZZB, chain B; UniProt: A0A0F8V8L2; (36)), and malarial parasite (*Plasmodium falciparum*, PDB ID: 2JKG, chain A; UniProt: Q8I2J4; (37)). Specific insertions, which are not present in mammalian profilin, are highlighted by *pink* in *Plasmodium*, by *orange* in *Leishmania*, and by *light brown* in Loki profilin sequences. *C*, superimposition of the profilins from human, *Plasmodium*, and Asgard archaea with the *Leishmania* profilin, when in complex with an actin monomer. The positions of *Leishmania*, malaria parasite, and Lokiarchea-specific insertions in the structures are indicated with *red*, *pink*, and *light brown arrows*, respectively. A view of 45° was selected to better visualize the locations of the insertions in all three profilins.

the complex with profilin is very similar to the structure of actin in the previously determined from bovine and Archaea profilin–actin complexes (Fig. S1A). Interestingly, the actin-binding interface of profilin is not particularly well conserved between the *Leishmania* and mammalian proteins, apart from certain key residues discussed later in the text (Fig. S1B).

The most striking difference of *Leishmania* and *Trypanosoma* profilins compared with the profilins from other organisms is the presence of a ~20 amino acid insertion (28, 29). In our crystal structure, this insertion is located between the last β-strand and C-terminal α-helix of the profilin fold, and it adopts an α-helical conformation flanked by small stretches of flexible linker sequences. Interestingly, the α-helical part of the

loop interacts with the target binding cleft of actin, between actin subunits 1 and 3 (Fig. 1, *A* and *B*). The loop insertion appears to be specific for trypanosomatid profilins. This is because although also malaria parasite and Loki archaea profilins contain insertions as compared with mammalian profilins, those are located at different positions of the profilin fold, and interact with different surfaces of an actin monomer (Fig. 1, *B* and *C*). Based on molecular dynamics simulation experiments, the specific loop in *Plasmodium* profilin interacts mainly with the barbed end side of subdomain 3 surface, whereas in the crystal structure, the Loki loop targets the same subdomain but at the back surface. Thus, the crystal structure of *Leishmania* profilin–actin complex shows that

trypanosomatid profilins interact with actin monomers through a mechanism that is distinct from those of profilins from other organisms.

Trypanosomatid profilins harbor a WH2-like actin-binding motif

More detailed analysis of the binding mode of trypanosomatid-specific loop of profilin with actin shows that two leucines, Leu115 and Leu119, of the α-helical region of the insertion associate with the hydrophobic pocket of actin formed by residues Ile345, Leu346, Leu349, and Tyr143 in the target binding cleft located between subdomains 1 and 3 (Fig. 2, *A* and *B*). Interestingly, the position of α-helical insertion (α-helix 4) of *Leishmania* profilin on the actin monomer and the mechanism by which it interacts with the surface of actin are similar to that of the WH2 domain (Fig. 2*C*). WH2 domain is a short ubiquitous motif of 15 to 20

amino acids present in many regulators of actin dynamics. These include, for example, actin filament nucleation-promoting factors WASP, N-WASP, and WAVE complex, as well as proteins catalyzing actin filament nucleation/polymerization, such as Leiomodin, Spire, Cobl, and Ena/VASP (38). Typically, WH2 domains utilize two conserved leucines or isoleucines in their α-helical region for interactions with actin, and these hydrophobic residues are also present in the α-helical region of the loop insertion of *Leishmania* profilin. However, this α-helix in LmProfilin is slightly shorter as compared with the majority of canonical WH2 domains (Fig. 2*D*). Moreover, in most WH2 domains, the α-helix is followed by another region called LKKV or LRRV motif (Leu-Lys/Arg-Lys/Arg-Val), which, however, is absent from *Leishmania* profilin. Interestingly, also other regulators of actin that interact with the barbed end surface apply similar mechanistic properties in their mode of actin binding. For example, the
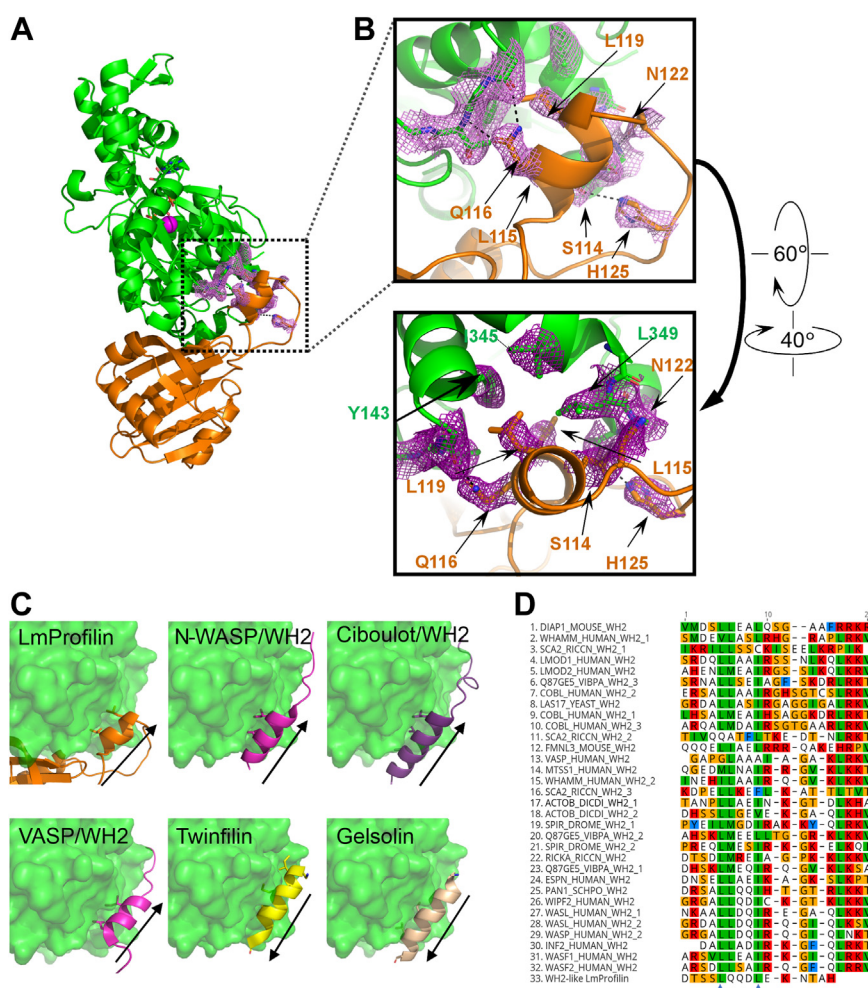

Figure 2. Trypanosomatid parasites harbor a WH2 domain–like α-helical insertion. *A*, side view of the *Leishmania* profilin–actin complex showing the interactions of profilin α-helical insertion with actin. *B*, magnified view of the interactions of *Leishmania* profilin α-helix with actin. Key residues contributing to the interaction are marked by *sticks* and labeled with the same color as the corresponding protein molecule. Electron density map (2$F_0 - F_C$, σ = 1.0) is also shown for selected residues. *C*, comparison of α-helical regions of *Leishmania* profilin insertion (Protein Data Bank [PDB] ID: 8C47), selected WH2 domains (N-WASP/WH2 [PDB ID: 2VCP; (74)], Ciboulot/WH2 [PDB ID:1SQK; (75)], and VASP/WH2 [PDB ID: 2PBD; (76)]), as well as twinfilin (PDB ID: 3DAW; (77)) and gelsolin (PDB ID:1T44; (78)). The positions of key hydrophobic residues involved in actin binding are shown. *Arrows* indicate the direction of polypeptide chain from the N-terminus to the C-terminus of α-helix. *D*, multiple sequence alignment of selected WH2 domains and the α-helical insertion of *Leishmania* profilin. The critical hydrophobic residues mediating actin monomer binding in WH2 domains are indicated with *blue arrowheads*. WH2, WASP homology-2 domain.

ADF-H fold of cofilin, gelsolin, and twinfilin contains an α-helix, which inserts in a similar fashion to the target binding cleft between actin subdomains 1 and 3. However, in contrast to the canonical WH2 domains and the α-helical insertion of *Leishmania* profilin, the α-helices in these proteins have opposite orientation. In cofilin, twinfilin, and gelsolin domains, the N-terminus of the α-helix is facing toward the pointed end of actin, whereas in the WH2 domains and in the α-helical insertion of *Leishmania* profilin, the N-terminus of α-helix is facing toward the barbed end of actin (Fig. 2*C*). Thus, different regulators of actin have found similar ways to interact with actin monomers through convergent evolution.

We next examined the role of the WH2 domain–like structural motif (hereafter termed the "WH2-like motif") in actin monomer binding by LmProfilin. For these experiments, we generated five mutant versions of LmProfilin and examined their binding to *L. major* ATP–actin monomers by isothermal titration calorimetry (ITC). In the mutant versions of profilin, the entire WH2-like motif was deleted (LmProfilin-ΔWH2), or the two conserved leucines of WH2-like motif in contact with actin were replaced by serines (LmProfilin-WH2-SS). Moreover, we introduced two mutations (LmProfilin-K68A and LmProfilin-K86E) to the "main" actin-binding interface, which is conserved in all profilins. The equivalents of these two mutations in other organisms were reported to affect actin monomer binding to different extents (39). Finally, we introduced a mutation to the putative polyproline-binding site of the protein (LmProfilin-Y6A), which is not in contact with actin monomer in our structure, to confirm that this mutation (used in other assays later) does not affect profilin's interaction with actin, for example, by disrupting its proper folding (Fig. 3*A*). ITC experiments showed that the interaction between LmActin with LmProfilin produced an exothermic reaction, and the binding isotherms were best fit to one-site binding model. WT LmProfilin and LmProfilin-Y6A mutant bound ATP-actin monomers with high affinity (K_d ∼90 nM, Figs. 3, *B* and *C* and S2), whereas mutations at the main binding interface either completely abolished actin binding (LmProfilin-K86E) or resulted in a very low affinity binding to LmActin (LmProfilin-K68A; K_d ∼3 μM) (Figs. 3*C* and S2). Interestingly, the mutant proteins in which the key actin-interacting residues of the WH2 motif were substituted by serines, or harbored complete deletion of the motif, still bound actin monomers, although with ∼25-fold reduced affinity as compared with the WT profilin (Figs. 3, *B* and *C* and S2).

Together, the structural and mutagenesis data provide evidence that LmProfilin harbors an α-helical insertion, which interacts with the hydrophobic cleft between actin subdomains 1 and 3 in a similar orientation as the WH2 domains. The WH2-like motif is not essential for interaction of *Leishmania* profilin with monomeric actin but increases the affinity of profilin for actin. Importantly, this insertion and its key actin-binding residues are conserved in *Leishmania* and *Trypanosoma* parasites, as well as in other trypanosomatids (Fig. S3), indicating that profilins from all trypanosomatid species apply the unique WH2-like motif to regulate actin dynamics.

Leishmania profilin binds proline-rich proteins and catalyzes nucleotide exchange on actin

Most profilins catalyze nucleotide exchange on actin monomers, and a recent study provided evidence that *L. donovani* profilin can accelerate nucleotide exchange on rabbit muscle actin to some extent (30). To examine the possible effects of LmProfilin on the rate of nucleotide exchange of LmActin monomers, we monitored the ATP-ATTO-488 fluorescence anisotropy kinetics in the presence of actin and WT/mutant profilins using the approach described (40). Unlike rabbit muscle actin, LmActin monomers do not efficiently exchange their bound nucleotide for ATP-ATTO-488 (Fig. 4*A*). The presence of *Leishmania* profilin lifts this inhibition and promotes rapid nucleotide exchange in a dose-dependent manner. This effect is observed for about 400 to 700 s, after which anisotropy signals slowly decrease instead of reaching steady-state values (Fig. 4*B*). Since injecting an additional dose of ATP-ATTO-488 after the anisotropy signals have returned to low values does not result in the formation of a new peak, we interpret this effect as a possible gradual inactivation or unfolding of nucleotide-free monomeric magnesium–actin during the exchange reaction (Fig. S4, *A* and *D*) (41, 42). Please note that in the experimental conditions of nucleotide exchange assay, the concentrations of ADP and ATP-488-ATTO are very low, and there is no unlabeled ATP. Consistent with its lower affinity for actin, the ΔWH2 profilin mutant comparatively showed reduced nucleotide exchange efficiency. The K68A mutant has no exchange efficiency, demonstrating that the conserved actin-binding interface of profilin is essential for nucleotide exchange in the *Leishmania* protein (Fig. 4*C*). Interestingly, the interplay between actin and profilin seems to have coevolved, as yeast (*Saccharomyces cerevisiae*) profilin showed no efficiency in promoting *Leishmania* actin nucleotide exchange (Fig. S4*B*); conversely, the catalytic activity on rabbit actin monomers decreased progressively with the degree of divergence of the profilin (Fig. S4*C*).

Another important feature of profilins is their ability to bind to proline-rich proteins. Our structure shows that the polyproline-binding site is conserved in LmProfilin (Fig. S1*B*), and *L. donovani* profilin was recently reported to bind to polyproline peptides in an affinity chromatography assay. However, the authors did not measure the binding affinity of the interaction or map the residues critical for polyproline binding (30). Here, we used the change in intrinsic tryptophan fluorescence of profilin upon binding to poly-L-proline to determine the dissociation constant of LmProfilin from a polyproline decamer. Based on this assay, WT LmProfilin binds the poly-L-proline peptide with an affinity (K_d of 263.2 ± 34.8 μM) that is similar to the ones reported for the interaction between poly-L-proline decamer and *Acanthamoeba* and human profilins (43). Tyr6 in LmProfilin is located in the putative polyproline binding site, and mutation of the corresponding tyrosine in *Schizosaccharomyces pombe* reduces affinity to poly-L-proline and poorly complements the loss of profilin *in vivo* (39). Similarly, replacing this tyrosine by alanine in
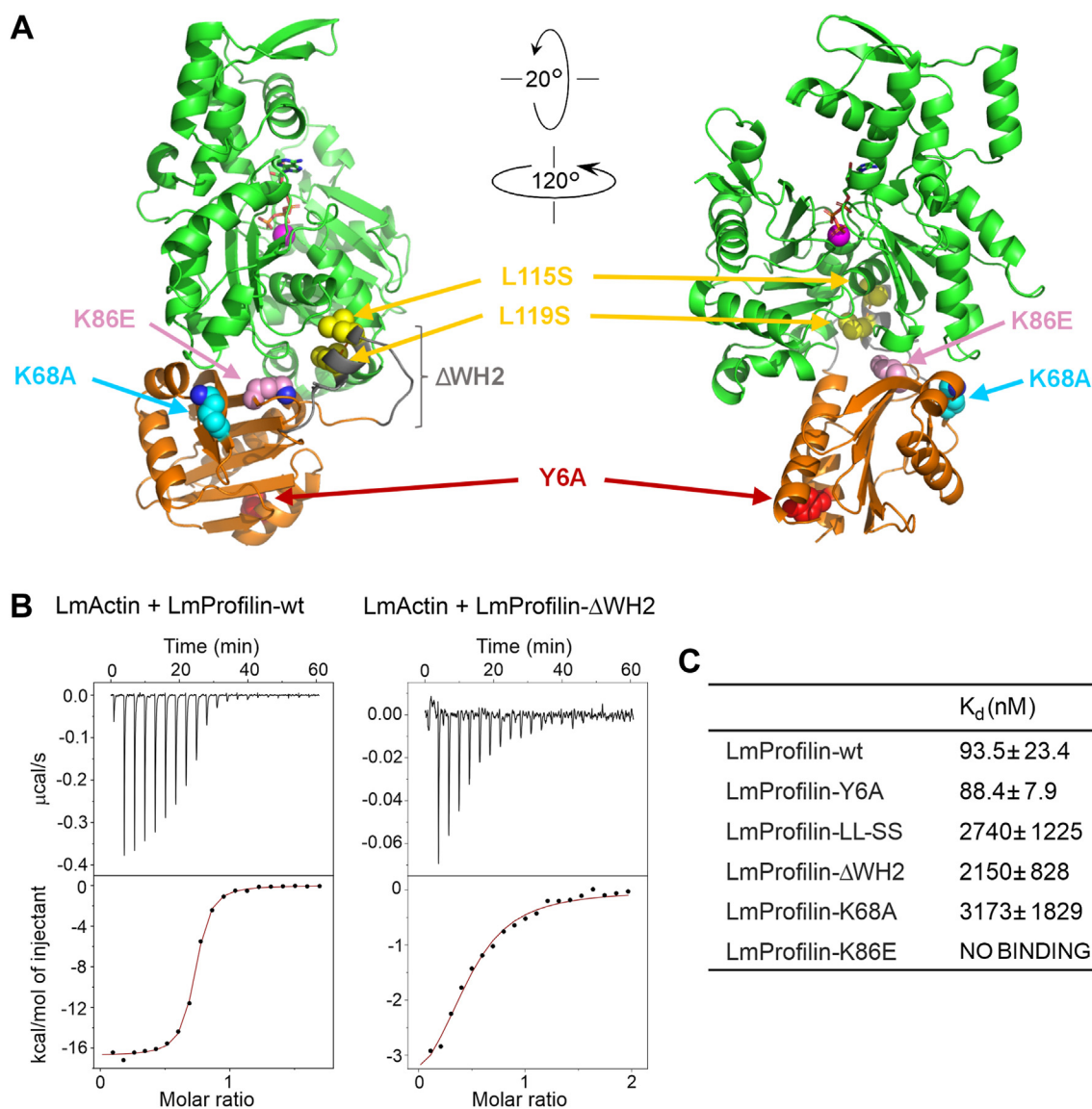
Figure 3. Site-directed mutagenesis reveals the roles of different protein motifs of *Leishmania* profilin in actin binding. *A*, the locations of amino acid residues that were mutated in *Leishmania* profilin (*yellow*, L115 and L119; *red*, Y6A; *gray*, deleted WH2 motif; *pink*, K86; and *cyan*, K68) are indicated in the profilin–actin complex (shown in two different orientations). *B*, examples of the data from the isothermal titration calorimetry assay. Baseline-corrected thermograms (*upper graphs*) and integrated data fit to one-site binding model (*lower graphs*) are shown. *C*, dissociation constants (K_d, in nM ± SD) of WT and mutant *Leishmania* profilins from *Leishmania* ATP–actin monomers, obtained from three independent ITC experiments for each protein. ITC, isothermal titration calorimetry.

LmProfilin (LmProfilin-Y6A) diminished binding to the poly-L-proline decamer to an undetectable level (Fig. 4D).

Collectively, these experiments demonstrate that LmProfilin binds polyproline-rich proteins and catalyzes the nucleotide exchange on actin monomers through interfaces that are conserved between human, yeast, and parasite profilins. However, efficient nucleotide exchange also relies on the WH2-like motif, which increases the affinity of LmProfilin to actin monomers.

Effects of Leishmania *profilin on formin-catalyzed actin filament assembly*

Profilins studied so far bind FH1 domains of formins and can hence deliver actin monomers to formin FH2 domains to enhance actin filament assembly (24). Because of the presence of the WH2-like motif in LmProfilin, we inspected whether the *Leishmania* profilin could be superimposed to the barbed end of the FH2 domain/actin cocrystal structure from yeast (44). Interestingly, whereas mammalian profilins can be superimposed to the barbed end face of the terminal actin subunit of the FH2 domain–bound filament end (45) (Fig. 5A), the WH2-like motif of LmProfilin makes pronounced steric clashes with the FH2 domain of formin (Fig. 5B). This suggests that *Leishmania* profilin might not be able to work together with formin in promoting actin filament assembly. We thus examined the effects of LmProfilin on actin polymerization of LmActin by using pyrene–actin polymerization assay.

Because an earlier study on *Leishmania* actin dynamics demonstrated that rabbit muscle actin can copolymerize with
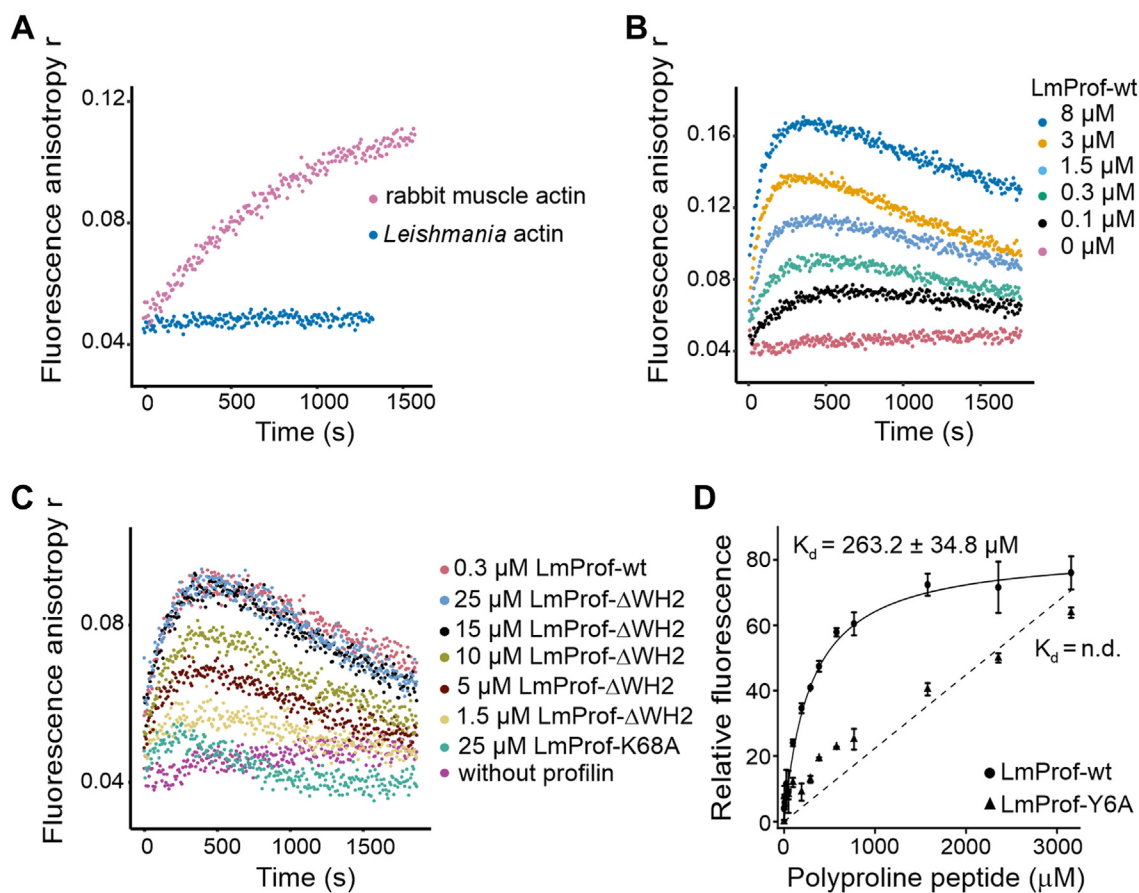
Figure 4. *Leishmania* profilin promotes nucleotide exchange on actin monomers and binds polyproline peptide through a conserved interface. *A*, ATP-ATTO-488 fluorescence anisotropy experiment to compare nucleotide exchange kinetics of *Leishmania* and rabbit muscle monomeric actins. *B*, ATP-ATTO-488 fluorescence anisotropy experiment to assess the effect of *Leishmania* profilin on nucleotide exchange kinetics of *Leishmania* monomeric actin. *C*, ATP-ATTO-488 fluorescence anisotropy experiment to compare the activities of WT and two mutants of *Leishmania* profilin (ΔWH2 and K68A). The data presented in *A–C* are representative of at least three independent experiments with similar results. *D*, tryptophan fluorescence assay to study the interaction of WT LmProfilin (LmProf-WT; *solid circles*) and LmProfilin-Y6A mutant (LmProf-Y6A; *solid triangles*) with a poly-ʟ-proline peptide. Different concentrations of a decamer poly-ʟ-proline peptide were mixed with 1 μM of profilins, and the relative fluorescence intensity was measured. Data points are shown in *symbols*, the fitting curves in *lines*, and the obtained K_d value for WT profilin—poly-ʟ-proline interaction is shown. The affinity of LmProfilin-Y6A to poly-ʟ-proline was too low to be detected by this assay (n.d. = not determined). The mean ± SD from three independent experiments is shown. LmProfilin, *Leishmania major* profilin.

Leishmania actin without drastically altering its assembly kinetics (18), we performed pyrene–actin polymerization experiments by using a mix of 95% LmActin and 5% pyrene-labeled rabbit muscle actin. As demonstrated before (18), purified LmActin polymerized readily in the absence of any actin filament nucleators, and this is most likely because of rapid spontaneous nucleation of this actin (Fig. 5*C*). Addition of WT LmProfilin inhibited spontaneous assembly of actin filaments, similar to other profilins. Also, the profilin mutant lacking the WH2-like motif inhibited spontaneous actin filament assembly, although to a lesser extent, most likely because of the lower binding affinity of this mutant profilin to actin (Figs. 3 and 5*C*). When the polymerization experiments were carried out in the presence of phalloidin-stabilized rabbit-actin seeds, the inhibition of actin assembly by profilin was mostly relieved, suggesting that LmProfilin does not significantly affect the incorporation of actin monomers to the pre-existing actin filament barbed ends (Fig. 5*D*). Interestingly, when the polymerization assay was carried out in the presence of FH1–FH2 fragment of *L. major* formin-B

(LmFormin), WT *Leishmania* profilin slowed down actin filament assembly by inducing an initial lag phase to filament assembly. In contrast, *Leishmania* profilin lacking the WH2-like motif had no detectable effect on actin filament assembly in the presence of *Leishmania* formin, even at high concentrations to compensate weaker affinity (Figs. 5*E* and S5, *A* and *B*). Please note that the *Leishmania* profilin lacking the WH2-like motif nevertheless bound proline-rich peptide, mimicking the formin FH1 domain, with very similar affinity compared with the WT profilin (Fig. S5*C*). Together, these data demonstrate that, similar to other profilins, LmProfilin inhibits spontaneous actin filament nucleation and maintains actin filament polymerization at filament barbed end. However, LmProfilin is not compatible in promoting actin filament assembly with formins because of the presence of WH2-like motif, which also makes a steric clash with formin at filament barbed end. Notably, the WH2-like motif is conserved in all trypanosomatid profilins suggesting a similar mode of action for profilin with formins in other trypanosomatid parasites.
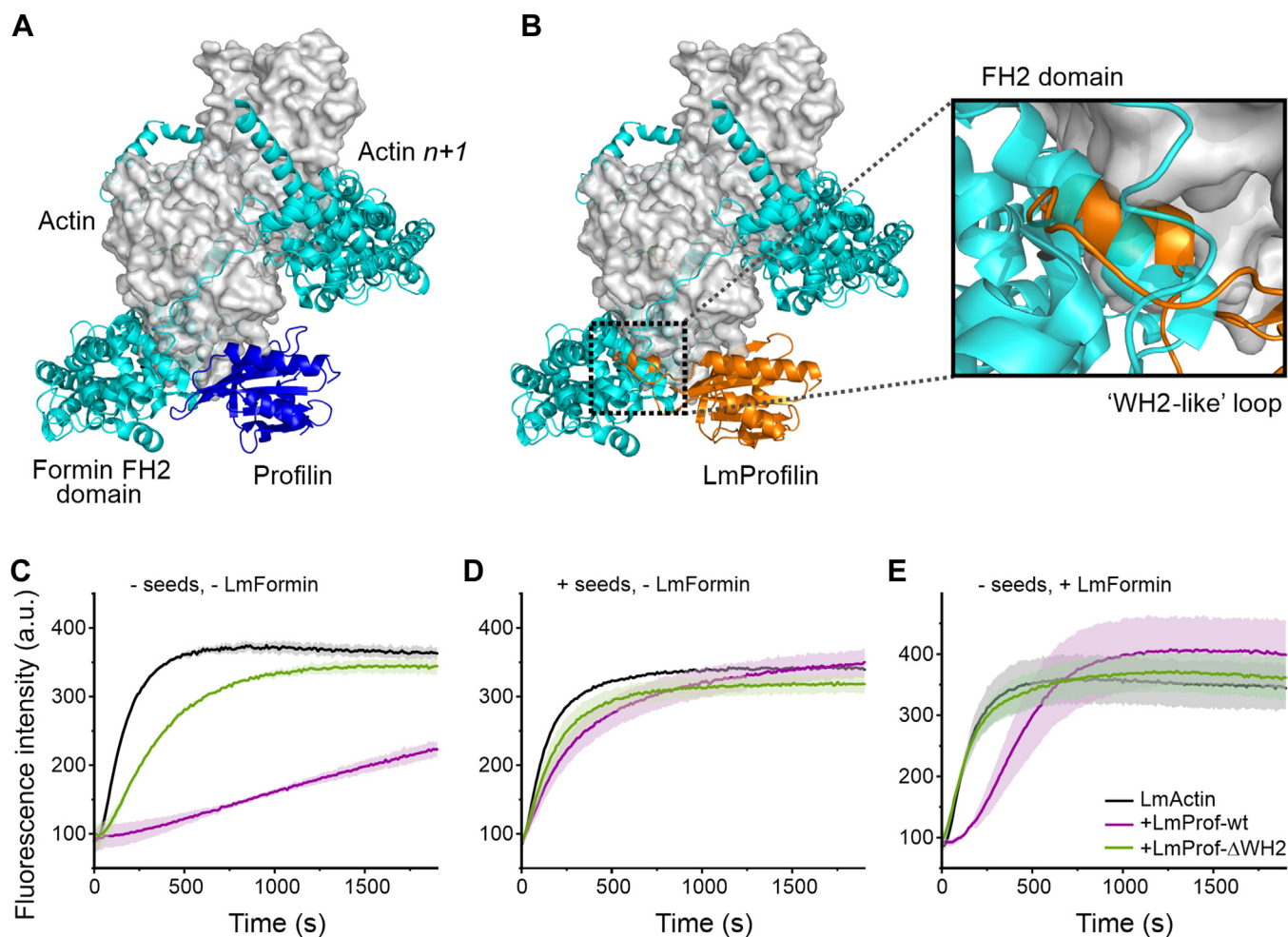
Figure 5. Effects of *Leishmania* profilin on formin-catalyzed actin filament assembly. *A,* human profilin-I (Protein Data Bank ID: 2BTF) can be fitted to the barbed end of the "terminal" actin subunit of the 2:2 FH2 domain:actin monomer structure (Protein Data Bank ID: 1Y64) without steric clashes. *B,* superimposition of the *Leishmania* profilin from our cocrystal structure to the FH2:actin structure results in major steric clashes between the profilin WH2-like motif and the FH2 domain. *C–E,* pyrene–actin polymerization assays to monitor the effects of WT (LmProf_WT; *purple curve*) and LmProfilin-ΔWH2 (LmProf_ΔWH2; *green curve*) on spontaneous actin filament assembly (*C*), on actin filament assembly from actin–phalloidin seeds (*D*), and on actin filament assembly induced by LmFormin FH1–FH2 fragment (*E*). Final concentrations of actin (95% LmActin, 5% rabbit-pyrene actin) and profilin were 3 μM, and the concentrations of LmFormin FH1–FH2 and phalloidin seeds were 0.05 μM and 0.03 μM, respectively. Each *curve* depicts the average of four independent experiments with SD shown in *lighter color*. FH2, formin homology 2; LmActin, *Leishmania major* actin; LmFormin, *L. major* formin-B; WH2, WASP homology-2 domain.

Interactions with actin and proline-rich proteins are important for the *in vivo* function of Leishmania *profilin*

To investigate the role of profilin and its different binding interfaces in parasites, we applied *Leishmania mexicana* as a model system. The *L. mexicana* and LmProfilins are >97% identical to each other at the amino acid level, and the residues mutated above are conserved between these two closely related parasites. We generated *L. mexicana* parasites expressing a range of profilin mutants (Figs. S6 and S7A). These include heterozygous (−/+) and homozygous (−/−) profilin knockouts as well as *L. mexicana* knockin strains expressing mutant versions of profilin. In the knockin strains, the remaining *profilin* allele of the heterozygous (−/+) strain was replaced by Myc-tagged WT or mutant LmProfilin. Based on Western blot using polyclonal anti-LmProfilin antibody, the expression level of WT Myc-LmProfilin in the knockin strain (*profilin -*/WT) was slightly reduced as compared with

the level of LmProfilin in the heterozygous (*profilin* −/+) strain (Fig. S7B). Because the polyclonal anti-LmProfilin antibody is likely to detect different mutant versions of LmProfilin with variable efficiency, we also probed the blot with anti-Myc antibody to compare the expression levels of WT and mutant profilins in the knockin strains. This demonstrated that all mutant Myc-LmProfilins were expressed either at similar or slightly higher protein levels as compared with the WT Myc-LmProfilin (Fig. S7B).

No effect on cell growth was observed in any profilin mutants, except a slight reduction in growth of the profilin null mutant (Fig. S8). Next, the effect of the profilin mutants on the uptake and trafficking of FM4-64, a lipophilic fluorescent dye, was examined. The flagellar pocket (FP) is the only known site for exocytosis and endocytosis in *Leishmania*, with FM4-64 initially accumulating at this point (46). FM4-64 is then trafficked to the endocytic system and finally to the tubular
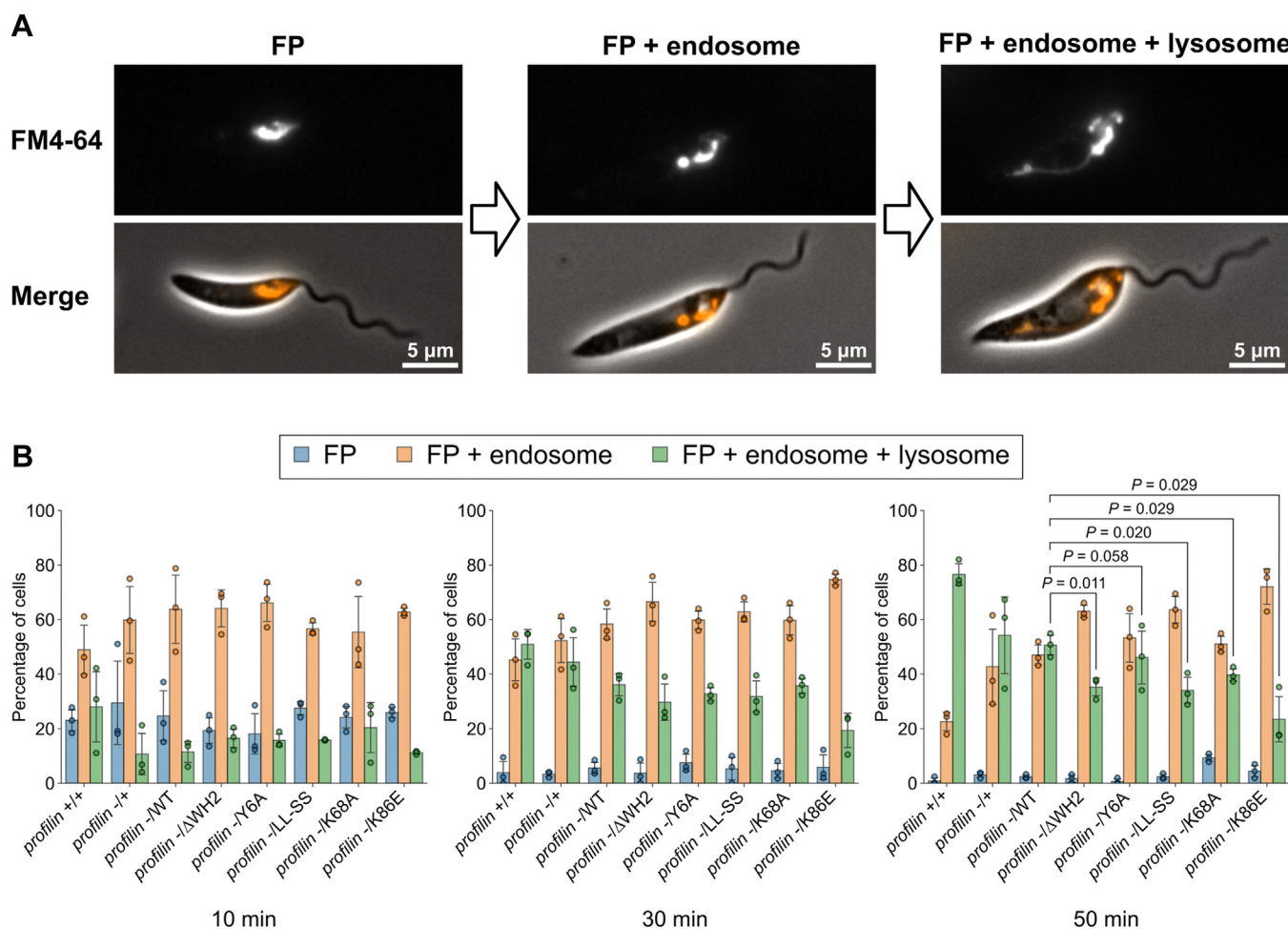
A

B

Figure 6. *Leishmania mexicana* parasites expressing profilin mutants have reduced FM4-64 trafficking. *A*, fluorescence and phase contrast microscopy images showing three major categories of FM4-64 localization after uptake into *L. mexicana* cells. *Left*, flagellar pocket (FP). *Middle*, FP and endosome. *Right*, FP, endosome, and lysosome. *B*, FM4-64 endocytosis assay with profilin WT and mutant *L. mexicana* strains. Cells were chilled on ice for 20 min and then pulsed with FM4-64 for 1 min before imaging at 10, 30, and 50 min time points. The number of cells in each of the three major categories of FM4-64 localization was counted at each time point. Data represent mean ± SD (n = 3 independent experiments). The *dots* represent individual measurement from three independent experiments (33–62 cells were counted in each measurement). *p* Values calculated using two-tailed Welch's *t* test.

lysosome, which runs along the anterior–posterior axis of the cell (Fig. 6*A*). We assessed the extent of uptake of FM4-64 for each profilin mutant and found a slower progression of FM4-64 trafficking in all profilin mutants compared with the WT profilin strain (*profilin* -/WT; Fig. 6*B*). The reduction of FM4-64 trafficking was slight in the proline-binding mutant (*profilin* -/Y6A) but somewhat more pronounced in the WH2 motif deletion (*profilin* -/ΔWH2) and the LL-SS (*profilin* -/LL-SS) mutants. There was also a significant reduction in FM4-64 trafficking in the actin-binding interface mutants, especially the K86E mutant (*profilin* -/K86E). Together, these experiments demonstrate that in *L. mexicana*, profilin is not essential for viability in laboratory conditions but is important for efficient endocytic trafficking. These results suggest that efficient endocytic trafficking is not critical for growth or viability of parasites when cultured in rich media. Importantly, the rescue experiments also revealed that profilin's ability to bind actin monomers and polyproline-rich proteins as well as the presence of functional WH2-like motif contribute to its role in endosomal trafficking.

Discussion

By determining the co-crystal structure of LmProfilin–actin complex, combined with biochemical work and studies on live parasites, our work uncovers the molecular principles by which actin dynamics are regulated by profilin in trypanosomatid parasites. This study also reveals important differences in the mechanisms by which trypanosomatid profilins associate with actin, as compared with the actin–profilin interactions of other organisms studied so far.

Our results provide evidence that the basic principles by which profilins interact with actin monomers are conserved across the eukaryotic domain. Similarly to eukaryotic profilins characterized so far, LmProfilin binds to the barbed end surface of actin, interacts with polyproline motifs, and inhibits spontaneous actin filament nucleation (Figs. 1, 4 and 5). Moreover, the "main" actin-binding interface of profilin is conserved in evolution from mammals to trypanosomatid parasites. The principles of actin monomer binding are also conserved in even more distant profilins from Asgard archaea, whereas the mechanism by which archaea profilins associate

with polyproline appears divergent from eukaryotic profilin (36, 47). However, in contrast to other profilins characterized so far, LmProfilin also harbors a WH2 domain–like insertion, which contributes to actin binding. In this context, it is important to note that also *Plasmodium* profilin harbors a structural insertion composed of two β-strands (35, 48, 49). This insertion is important for malaria parasite motility, but it is located in a topologically different position of the protein and, based on molecular dynamics simulation experiments, interacts with a different interface of actin as compared with the α-helical WH2-like motif of *Leishmania* profilin.

Our structural and biochemical work provides evidence that the WH2-like motif of *Leishmania* profilin increases its affinity for actin monomers and helps to catalyze nucleotide exchange on actin monomers. However, whether the WH2-like motif contributes to nucleotide exchange simply by increasing LmProfilin's affinity for actin monomers, or if it accelerates nucleotide exchange through a more specific mechanism, remains to be elucidated by more extensive mutagenesis analysis. Interestingly, *Leishmania* profilin also inhibits formin-mediated actin filament assembly through a mechanism that is dependent on the presence of the WH2-like motif, which makes a steric clash with the FH2 domain when superimposed into the yeast FH2 domain–actin structure. However, whether the WH2-like motif of LmProfilin inhibits formin-catalyzed filament assembly because of this steric clash or simply by increasing profilin's affinity for actin monomers remains to be shown. This is because also other profilins, including the ones from *Toxoplasma* and *Plasmodium* that do not harbor similar WH2-like motifs, inhibit formin-catalyzed actin filament assembly to different degrees (50, 51).

It is interesting to note that in other organisms many activators of the Arp2/3 complex harbor WH2 domains (38), and it is possible that trypanosomatid profilins predominantly work together with the Arp2/3 complex to promote actin filament assembly. This is also consistent with the phenotypes of *Leishmania* profilin knockout and knockin studies. Previous study on *L. donovani* heterozygous profilin mutant (30), and our present work on *L. mexicana* parasites expressing profilin mutants, demonstrated that profilin in trypanosomatid parasites is important for endocytic trafficking. Both endocytic internalization as well as endosomal sorting are processes that rely on the Arp2/3 complex nucleated and branched actin filament networks (52). Arp2/3 complex activation during endocytic internalization is mainly catalyzed by WASP family proteins (53), whereas the Arp2/3 activation in endocytic sorting is catalyzed by the WASH protein complex (54, 55). *Leishmania* genomes do not harbor clear homologs of WASP, but these organisms appear to express a protein, which displays weak sequence homology to the Arp2/3-interacting WASH-1 subunit of the WASH complex. Consistently, depletion of profilin results in defects in endosomal sorting, rather than endocytic internalization in *Leishmania* species. Our knockin studies provided evidence that interactions with actin and polyproline-rich proteins as well as the presence of a functional WH2-like motif are important for the function of *Leishmania* profilin in endocytic sorting. Thus, in addition to actin, profilin must also be able to

interact with proline-rich proteins during endocytosis. It is important to note that endocytic Arp2/3 activators, including the subunits of the WASH complex, contain proline-rich segments, which are likely to bind profilin (56).

There are, however, important open questions about regulation of actin filament assembly in trypanosomatid parasites. In addition to the Arp2/3 complex, these parasites express formins. In animals and fission yeast, Arp2/3 and formins assemble functionally distinct actin filament arrays, were shown to compete for a limited pool of actin monomers, and profilin having an important role in controlling the balance between Arp2/3- and formin-catalyzed actin filament assembly (57, 58). Thus, in the future, it will be important to study the roles of the Arp2/3 complex and formins during different cellular processes and developmental stages of *Leishmania* parasites. Because *Leishmania* formins harbor proline-rich FH1 domains, it is likely that at least under certain circumstances *Leishmania* profilin can also deliver actin monomers to formins. It is, therefore, possible that the "formin-inhibitory effect" of *Leishmania* profilin can be controlled by interactions with other proteins or through specific post-translational modifications of profilin. Finally, it is interesting to note that both *Leishmania* actin and especially ABPs display notable differences, both in their biochemistry and structures, compared with human actin and ABPs. Because actin is essential for viability of trypanosomatids (12), these differences, including the peculiar structural mechanism of *Leishmania* profilin–actin interaction identified here, could be applied for designing specific inhibitors against pathogenic trypanosomatid parasites.

Experimental procedures

Cloning

The gene sequence of WT LmProfilin (LmjF.32.0520) was taken from TriTrypDB database, codon optimized for bacterial expression, synthetized by TWIST Bioscience, and cloned into 3C/Precision cleavable double-tagged (Hisx6-glutathione-*S*-transferase [GST]) plasmid pCoofy3, a gift from Sabine Suppmann (Addgene plasmid #43983; http://n2t.net/addgene:43983; Research Resource Identifier [RRID]: Addgene_43983) (18, 59). The mutants were prepared by site-directed mutagenesis (see Tables S2 and S3 for details) following the QuikChange site-directed protocol (Agilent). For generation of knockin cell lines, the pPLOT blast-mNG-blast plasmid was generated with recoded WT and mutant profilin genes (synthetized by TWIST Bioscience) between the HindIII and SacI sites. A gene fragment encoding LmForminB (amino acids 536–1193) was codon optimized, synthesized by Integrated DNA Technologies, and cloned into the same pCoofy3 plasmid.

Protein purification

L. major actin (LmActin; TriTrypDB ID: LmjF.04.1230) fused with human-β-thymosin and a His10x tag at the C terminus of actin was expressed in ExpiSf9 insect cells using the baculovirus system and subsequently purified by nickel–nitrilotriacetic acid

(Ni–NTA) affinity chromatography followed by gel filtration, as previously described (18). Please note that, similarly to our previous study (18), we used the amino acid sequence of LmActin that corresponds to UniProt entry Q9U1E8 and to TriTrypDB: LmjF.04.1230 entry in TriTrypDB. There is also another entry, P45520, reported in 1995 that is 100% similar and 99% identical (disagreements Q9U1E8 [93]EL[94], P45520 [93]DV[94]). Pure protein was flash-frozen in liquid nitrogen for long-term storage or immediately further processed. β-thymosin-His10x tag was removed by cleavage with α-chymotrypsin. After quenching of cleavage reaction with PMSF, polymerization of LmActin was induced by adding EGTA and $MgCl_2$, and filamentous actin was pelleted at $124,759g$ at 10 °C for 1 h. Actin pellets were washed and resuspended in G-buffer (2 mM Tris [pH 7.5], 0.5 mM β-mercaptoethanol, 0.2 mM $CaCl_2$, and 0.2 mM ATP) to a final concentration of ~0.8 mg/ml and dialyzed against G-buffer. Before assays, LmActin was ultracentrifuged for 1 h at $124,759g$ at 4 °C, and the upper two-thirds were collected to ensure only the presence of monomeric LmActin (18). The final LmActin concentration ranges between 14 and 19 μM. LmProfilin (TriTrypDB ID: LmjF.32.0520) WT and mutants were expressed as fusion proteins with an N-terminal double tag (His6x-GST). The recombinant proteins were purified using an approach reported before (18). Briefly, *Escherichia coli* BL21(DE3) (Merck Millipore) cells were grown at 22 °C in LB autoinduction media (AIMLB0210; Formedium) supplemented with kanamycin (20 μg/ml) for ~24 h. After lysis, recombinant proteins were first purified using a Ni–NTA column (GE HealthCare), and the His-GST tag was removed by cleavage with 3C-PreScission protease and subsequent incubation with Ni^{2+} beads to remove the uncleaved protein and the tag from the solution. The recombinant profilins were further purified by gel filtration, concentrated using Amicon Ultracentrifugal filters with molecular weight cutoff (MWCO) of 3 kDa (Merck), aliquoted, flash-frozen in liquid nitrogen, and stored at –75 °C until use. For LmFormin (TriTrypDB ID: LmjF.24.1110), the construct consisted only of the FH1–FH2 domains and the C-tail (amino acids 536–1193) fused to a His6x-GST tag at the N terminus of the formin fragment. Expression and purification of the polypeptide was carried out in a similar way as described previously and elsewhere (60), with slight modifications. Bacterial cells were harvested by centrifugation and lysed by sonication in the presence of lysozyme (0.5 mg/ml), DNase I (0.1 mg/ml), and protease inhibitors. The lysate was clarified by centrifugation and by passing through a 0.45 μm filter before loading it into a Ni–NTA column connected to an AKTA Pure instrument (GE Healthcare). After the protein binding to Ni–NTA beads, the column was washed with binding buffer (50 mM Tris–HCl, 300 mM NaCl, 10 mM imidazole, 3% glycerol, pH 7.5), and the protein was eluted with a linear gradient until reached 100% of elution buffer (50 mM Tris–HCl, 300 mM NaCl, 250 mM imidazole, 3% glycerol, pH 7.5). Peak fractions were pooled and concentrated by Amicon MWCO 50 kDa filters and loaded into a HiLoad 16/600 Superdex 200 column equilibrated with 20 mM Hepes (pH 8.0) buffer, 50 mM NaCl, 3% glycerol, for gel filtration chromatography. Fractions corresponding to the desired protein were pooled and cleaved with 3C PreScission protease for 1 h at 4 °C with gentle rotation. Glutathione-

sepharose 4 beads (GE Healthcare) were added to remove the cleaved tags and noncleaved protein for another 2 h at 4 °C in a column under gravity flow. Protein was aliquoted and flash frozen for storage at –75 °C until further use. Yeast profilin (Pfy1p) and mouse profilin-1 (PROF1) were expressed in Rosetta2(DE3)pLysS cells as fusion proteins with an N-terminal tag (6xHis-TEV). The recombinant proteins were batch purified on Ni-Sepharose beads 6 Fast Flow (GE Healthcare) and eluted with 6xHis-TEV protease. Proteins were concentrated by Amicon filters MWCO 10 kDa, dialyzed for 2 h at 4 °C against storage buffer (20 mM Hepes [pH 7.5], 50 mM KCl, and 6% glycerol) and flash frozen for storage. Rabbit muscle actin was purified as described (61).

Crystallization and structure determination

LmProfilin and LmActin were mixed at ~1:1 M ratio and 4.5 to 6.5 mg/ml concentration for sitting drop crystallization at Crystallization core facility (Institute of Biotechnology, HiLife). Hits were obtained from 0.1 M Bis–Tris (pH 5.5), PEG4000 26% (w/v), and 0.2 M NaCl. Crystals were fished and cryoprotected with 15 to 20% glycerol for shipment to remote data collection at Diamond Light Source (beamline I03; Oxfordshire). The data were collected with 0.1° oscillation per frame and 0.010 s exposure time at a wavelength of 0.9762 Å and processed with auto-PROC package, which utilizes XDS and AIMLESS for indexing, integration, and scaling of the data (62–65). Next, we used the sequences of LmActin and LmProfilin as inputs for homologous model search molecular replacement with ARP/wARP classic model building web service (66, 67) (https://arpwarp.embl-hamburg.de/). After the initial solution, the model was finalized with manual curation in Coot (68) and rounds of refinement in PHENIX 1.20.1_4487 (69). In the regions where the density was poor (*e.g.*, chain B residues 233–236), we used the previously determined structure of LmActin (Protein Data Bank ID: 7Q8B) as a guide to trace the protein chain. Nevertheless, we could not resolve the D-loop (chain B residues 40–51), probably because of its flexible nature, and hence, there is a gap in the structure. Please note that we modeled also the side chains of those amino acids, for which we did not detect density for all atoms.

ITC

ITC assays were performed in a Microcal-PEAQ instrument (Malvern Panalytical). Both LmActin and the proteins used for titration (WT LmProfilin and mutant versions) were dialyzed to G-buffer and degassed under vacuum for 30 min before each experiment. Titrations were done at 22 °C with LmActin (14–19 μM) loaded in the sample cell (250 μl) and injecting the ligand (150 μM in the syringe), with an initial 0.5 μl injection followed by nineteen 2 μl injections, each lasting 4 s and with 180 s of spacing between injections. The obtained thermograms were analyzed with the MicroCal PEAQ Analysis software using the single set of sites model to fit the curves. Heat because of dilution was corrected by control injections of LmProfilin into buffer.

Tryptophan fluorescence assay

LmProfilins (WT or mutants) at a final concentration of 1 μM were mixed at room temperature (RT) with different

concentrations (at final concentrations from 3 to 3156 μM) of a decamer poly-L-peptide (CASLO ApS) in 20 mM Hepes (pH 8.0), 50 mM NaCl buffer in a final volume of 110 μl. Change in intrinsic fluorescence intensity was measured in a Cary Eclipse Spectrophotometer (Agilent Technologies) at an excitation wavelength of 295 nm and range emission from 300 to 500 nm (5 nm slit width). The normalized maximum intensity fluorescence (determined as the average of the five highest intensities) was plotted against the peptide concentration. To calculate the dissociation constant (K_d), the data were analyzed in OriginPro and fit by nonlinear least-squares method using the OneSiteBind function.

Pyrene–actin polymerization assays

Polymerization of LmActin was analyzed by the increase in fluorescence of pyrene–actin measured in a Cary Eclipse Fluorescence spectrophotometer at RT, with an excitation wavelength of 365 nm and an emission wavelength of 407 nm. Before each experiment, LmActin was centrifuged at 124,759g for 60 min at 4 °C to remove possible oligomers. For each polymerization reaction, 60 μl of 1:10 final volume of 10× initiation buffer (20 mM Hepes, pH 7.4, 0.1 M KCl, 0.1 mM EGTA, 1 mM MgCl$_2$, and 0.2 mM ATP) containing either WT LmProfilin, or mutant LmProfilin ΔWH2 (in a final concentration of 3 μM), with or without LmFormin FH1–FH2 and phalloidin-stabilized actin seeds (at final concentrations of 0.05 μM and 0.03 μM, respectively) and G-buffer if needed, was combined with 60 μl of monomeric LmActin (5% pyrene-rabbit actin from Cytoskeleton, Inc) in G-buffer to yield a final concentration of 3 μM of actin in a final volume reaction of 120 μl. For the titration assays, the same conditions and concentrations for LmActin and LmFormin were used in combination with different concentrations (1, 3, 5, and 10 μM) of WT LmProfilin or LmProfilin ΔWH2.

Nucleotide exchange assay

Rabbit muscle or LmActins were incubated with a 1:10 volume of 10× exchange buffer (100 mM Tris [pH 8.0], 2.5 mM EGTA, 1 mM MgCl$_2$, and 0.2 mM ADP) for 5 min on ice and then dialyzed against G-ADP buffer (5 mM Tris [pH 7.5], 0.1 mM MgCl$_2$, 0.02 mM ADP, and 0.5 mM DTT) for 1 h at 4 °C. All exchange experiments reported in this article were initiated by incubation of G-actin (1 μM) with N^6-(6-Amino) hexyl-ATP-ATTO-488 (0.1 μM; Jena Bioscience, ref. NU-805-488) in G + ME buffer (5 mM Tris [pH 7.5], 0.1 mM CaCl$_2$, 0.5 mM DTT, 1 mM EGTA, and 1 mM MgCl$_2$) at RT. Anisotropy values were recorded by excitation at 504 nm and emission at 521 nm on a Safas Xenius XC spectrofluorimeter (Safas Monaco), using a kinetic acquisition mode available on the version 7.8.13.0 of the SP2000 software. Data were plotted with RStudio.

Leishmania *cell culture and generation of profilin knock in/out mutants*

L. mexicana promastigotes (WHO strain MNYC/BZ/1962/M379), expressing Cas9 nuclease and T7 RNA polymerase were grown at 28 °C in M199 medium with 10% fetal calf serum, 40 mM Hepes–NaOH (pH 7.4), 26 mM NaHCO$_3$, and 5 μg/ml hemin (70). The authenticity of the cell lines was validated by genome and mRNA sequencing. The cell lines were monitored for contamination, including mycoplasma contamination, through DNA staining and microscopy during data capture. Cells were maintained in logarithmic growth. Profilin knockout constructs and guide RNAs were generated as described (70). LeishGEdit was used to design primers for use with the knockout plasmid pTNeo. The plasmids (pPL1795-1800) were used as templates to generate knockin constructs that were transfected alongside the profilin 5′ guide RNA template (Fig. S6). The knockout and knockin constructs were transfected into 1×10^7 cells resuspended in transfection buffer (200 mM Na$_2$HPO$_4$, 70 mM NaH$_2$PO$_4$, 15 mM KCl, 150 mM Hepes [pH 7.3], and 1.5 mM CaCl$_2$), using programme X-001 on a Amaxa Nucleofector IIb. After electroporation, cells were transferred into 10 ml of M199 and incubated at 28 °C. After ~6 h, transfected cells were selected with appropriate drug (blasticidin—5 μg/ml, G418—20 μg/ml) for 5 to 10 days before subculturing of successful transformants. To confirm the knockout/knockin of profilin in mutant cells, PCR was performed on genomic DNA extracted using DNeasy Blood & Tissue kit (Qiagen).

Endocytosis assays

A total of 5×10^6 cells of log-phase *L. mexicana* promastigotes were incubated in M199 medium on ice for 20 min before final concentration of 5 μg/ml FM4-64 (Invitrogen; from a 1000 μg/ml stock solution in dimethyl sulfoxide) was added for 1 min at RT. Cells were centrifuged at 800g for 3 min at RT, resuspended in 600 μl of prewarmed M199 at 28 °C, and then divided into three tubes of 200 μl each. Each tube was incubated at 28 °C and at each time point (10, 30, and 50 min), one of the tubes was centrifuged at 800g for 1 min at RT to concentrate cells for imaging with a Zeiss ImagerZ2 microscope with a 63× numerical aperture 1.4 objective and Hamamatsu Flash 4 camera. Captured cells were categorized according to the FM4-64 localization (Fig. 6A; FP; FP and endosome; and FP, endosome, and lysosome).

Western blots

A total of 4×10^7 cells of log-phase *L. mexicana* promastigotes were harvested by centrifugation (800g for 7 min at RT). The cells were washed with 5 ml of PBS (137 mM NaCl, 2.7 mM KCl, 10 mM Na$_2$HPO$_4$, and 1.8 mM KH$_2$PO$_4$) and resuspended in 1 ml of ice-cold PBS with cOmplete, EDTA-free protease inhibitor cocktail (Roche). The cells were pelleted by centrifugation (10,000g for 2 min at RT) and resuspended in 200 μl of Laemmli buffer (2% SDS, 10% glycerol, 60 mM Tris–HCl, 50 mM DTT, pH 6.8) with cOmplete EDTA-free protease inhibitor cocktail. Cell lysates (approximately 4×10^6 cell equivalents, without heating) were loaded and subjected to electrophoresis on 15% SDS-polyacrylamide gels and transferred to a nitrocellulose membrane (GE Healthcare) in transfer buffer (25 mM Tris, 192 mM glycine,

and 20% methanol) without SDS. The membrane was blocked in 5% skim milk in Tris-buffered saline (20 mM Tris, 150 mM NaCl, pH 7.5) with 0.1% (w/v) Tween-20 (TBST) at RT for 1 h, then probed overnight at 4 °C with 1:500 dilution of guinea pig anti-LmProfilin antiserum (raised against recombinant LmProfilin by Pineda Antikörper-Service—see Fig. S7 for validation of the specificity of the antibody) or with mouse anti-myc-tag antibody (clone 9E10 hybridoma supernatant, grown in Sunter Laboratory; the antibody has been validated previously (71) and further optimized in the Sunter Laboratory) in blocking buffer. After washing with TBST, membranes were incubated at RT for 1 h with 1:1000 dilution of horseradish peroxidase–conjugated rabbit antiguinea pig IgG secondary antibody (Invitrogen; catalog no.: 61-4620, Lot no.: UK290200, RRID: AB_2533926; the antibody has been validated by the supplier), or with 1:2500 dilution of horseradish peroxidase–conjugated donkey antimouse IgG secondary antibody (Jackson ImmunoResearch; catalog no.: 715-035-150; Lot no.: 146022; RRID: AB_2340770; the antibody has been validated by the supplier) in blocking buffer, washed in TBST, and incubated with WesternBright Quantum (Advansta). The membrane was visualized by G:BOX Chemi XRQ instrument (Syngene).

Data availability

The data supporting the findings of the study are available in the article and supporting information. Other raw data generated in the study are available from the corresponding author on reasonable request.

Abbreviations—The abbreviations used are: ABP, actin-binding protein; FH1, formin homology 1 domain; FH2, formin homology 2 domain; FP, flagellar pocket; GST, glutathione-S-transferase; ITC, isothermal titration calorimetry; LmActin, *Leishmania major* actin; LmFormin, *Leishmania major* formin-B; LmProfilin, *Leishmania major* profilin; MWCO, molecular weight cutoff; Ni–NTA, nickel–nitrilotriacetic acid; RRID, Research Resource Identifier; RT, room temperature; TBST, Tris-buffered saline with Tween-20; WH2, WASP homology-2.

References

1. Mann, S., Frasca, K., Scherrer, S., Henao-Martinez, A. F., Newman, S., Ramanan, P., *et al.* (2021) A review of leishmaniasis: current knowledge and future directions. *Curr. Trop. Med. Rep.* **8**, 121–132
2. World Health Organization (2023) *Leishmaniasis*
3. Kaufer, A., Ellis, J., Stark, D., and Barratt, J. (2017) The evolution of trypanosomatid taxonomy. *Parasit Vectors* **10**, 287
4. Sunter, J., and Gull, K. (2017) Shape, form, function and *Leishmania* pathogenicity: from textbook descriptions to biological understanding. *Open Biol.* **7**, 170165
5. Zinoviev, A., and Shapira, M. (2012) Evolutionary conservation and diversification of the translation initiation apparatus in trypanosomatids. *Comp. Funct. Genomics* **2012**, 813718
6. Gull, K. (1999) The cytoskeleton of trypanosomatid parasites. *Annu. Rev. Microbiol.* **53**, 629–655
7. Berriman, M., Ghedin, E., Hertz-Fowler, C., Blandin, G., Renauld, H., Bartholomeu, D. C., *et al.* (2005) The genome of the African trypanosome *Trypanosoma brucei*. *Science* **309**, 416–422
8. de Souza, W., Meza, I., Martinez-Palomo, A., Sabanero, M., Souto-Padron, T., and Meirelles, M. N. (1983) *Trypanosoma cruzi*: distribution of fluorescently labeled tubulin and actin in epimastigotes. *J. Parasitol.* **69**, 138–142
9. Mortara, R. A. (1989) Studies on trypanosomatid actin. I. Immunochemical and biochemical identification. *J. Protozool* **36**, 8–13
10. Blanchoin, L., Boujemaa-Paterski, R., Sykes, C., and Plastino, J. (2014) Actin dynamics, architecture, and mechanics in cell motility. *Physiol. Rev.* **94**, 235–263
11. Lappalainen, P., Kotila, T., Jegou, A., and Romet-Lemonne, G. (2022) Biochemical and mechanical regulation of actin dynamics. *Nat. Rev. Mol. Cell Biol.* **23**, 836–852
12. Garcia-Salcedo, J. A., Perez-Morga, D., Gijon, P., Dilbeck, V., Pays, E., and Nolan, D. P. (2004) A differential role for actin during the life cycle of *Trypanosoma brucei*. *EMBO J.* **23**, 780–789
13. Tammana, T. V., Sahasrabuddhe, A. A., Bajpai, V. K., and Gupta, C. M. (2010) ADF/cofilin-driven actin dynamics in early events of *Leishmania* cell division. *J. Cell Sci.* **123**, 1894–1901
14. Gupta, C. M., Ambaru, B., and Bajaj, R. (2020) Emerging functions of actins and actin binding proteins in trypanosomatids. *Front. Cell Dev. Biol.* **8**, 587685
15. Kapoor, P., Kumar, A., Naik, R., Ganguli, M., Siddiqi, M. I., Sahasrabuddhe, A. A., *et al.* (2010) *Leishmania* actin binds and nicks kDNA as well as inhibits decatenation activity of type II topoisomerase. *Nucleic Acids Res.* **38**, 3308–3317
16. Akil, C., Kitaoku, Y., Tran, L. T., Liebl, D., Choe, H., Muengsaen, D., *et al.* (2021) Mythical origins of the actin cytoskeleton. *Curr. Opin. Cell Biol.* **68**, 55–63
17. Pollard, T. D. (2016) Actin and actin-binding proteins. *Cold Spring Harb. Perspect. Biol.* **8**, a018226
18. Kotila, T., Wioland, H., Selvaraj, M., Kogan, K., Antenucci, L., Jegou, A., *et al.* (2022) Structural basis of rapid actin dynamics in the evolutionarily divergent *Leishmania* parasite. *Nat. Commun.* **13**, 3442
19. Vizcaino-Castillo, A., Osorio-Mendez, J. F., Ambrosio, J. R., Hernandez, R., and Cevallos, A. M. (2020) The complexity and diversity of the actin cytoskeleton of trypanosomatids. *Mol. Biochem. Parasitol.* **237**, 111278
20. Goldschmidt-Clermont, P. J., Machesky, L. M., Doberstein, S. K., and Pollard, T. D. (1991) Mechanism of the interaction of human platelet profilin with actin. *J. Cell Biol.* **113**, 1081–1089

21. Eads, J. C., Mahoney, N. M., Vorobiev, S., Bresnick, A. R., Wen, K. K., Rubenstein, P. A., *et al.* (1998) Structure determination and characterization of *Saccharomyces cerevisiae* profilin. *Biochemistry* **37**, 11171–11181

22. Wolven, A. K., Belmont, L. D., Mahoney, N. M., Almo, S. C., and Drubin, D. G. (2000) *In vivo* importance of actin nucleotide exchange catalyzed by profilin. *J. Cell Biol.* **150**, 895–904

23. Watanabe, N., Madaule, P., Reid, T., Ishizaki, T., Watanabe, G., Kakizuka, A., *et al.* (1997) p140mDia, a mammalian homolog of *Drosophila* diaphanous, is a target protein for Rho small GTPase and is a ligand for profilin. *EMBO J.* **16**, 3044–3056

24. Chesarone, M. A., DuPage, A. G., and Goode, B. L. (2010) Unleashing formins to remodel the actin and microtubule cytoskeletons. *Nat. Rev. Mol. Cell Biol.* **11**, 62–74

25. Courtemanche, N. (2018) Mechanisms of formin-mediated actin assembly and dynamics. *Biophys. Rev.* **10**, 1553–1569

26. Chalkia, D., Nikolaidis, N., Makalowski, W., Klein, J., and Nei, M. (2008) Origins and evolution of the formin multigene family that is involved in the formation of actin filaments. *Mol. Biol. Evol.* **25**, 2717–2733

27. Funk, J., Merino, F., Venkova, L., Heydenreich, L., Kierfeld, J., Vargas, P., *et al.* (2019) Profilin and formin constitute a pacemaker system for robust actin filament growth. *Elife* **8**, e50963

28. Wilson, W., and Seebeck, T. (1997) Identification of a profilin homologue in *Trypanosoma brucei* by complementation screening. *Gene* **187**, 201–209

29. Osorio-Mendez, J. F., Vizcaino-Castillo, A., Manning-Cela, R., Hernandez, R., and Cevallos, A. M. (2016) Expression of profilin in *Trypanosoma cruzi* and identification of some of its ligands. *Biochem. Biophys. Res. Commun.* **480**, 709–714

30. Ambaru, B., Gopalsamy, A., Tammana, T. V. S., Subramanya, H. S., and Gupta, C. M. (2020) Actin sequestering protein, profilin, regulates intracellular vesicle transport in *Leishmania. Mol. Biochem. Parasitol.* **238**, 111280

31. Ambaru, B., Gangadharan, G. M., Subramanya, H. S., and Gupta, C. M. (2022) Profilin is involved in G1 to S phase progression and mitotic spindle orientation during *Leishmania donovani* cell division cycle. *PLoS One* **17**, e0265692

32. Schutt, C. E., Myslik, J. C., Rozycki, M. D., Goonesekere, N. C., and Lindberg, U. (1993) The structure of crystalline profilin-beta-actin. *Nature* **365**, 810–816

33. Fedorov, A. A., Pollard, T. D., and Almo, S. C. (1994) Purification, characterization and crystallization of human platelet profilin expressed in *Escherichia coli. J. Mol. Biol.* **241**, 480–482

34. Ezezika, O. C., Younger, N. S., Lu, J., Kaiser, D. A., Corbin, Z. A., Nolen, B. J., *et al.* (2009) Incompatibility with formin Cdc12p prevents human profilin from substituting for fission yeast profilin: insights from crystal structures of fission yeast profilin. *J. Biol. Chem.* **284**, 2088–2097

35. Moreau, C. A., Bhargav, S. P., Kumar, H., Quadt, K. A., Piirainen, H., Strauss, L., *et al.* (2017) A unique profilin-actin interface is important for malaria parasite motility. *PLoS Pathog.* **13**, e1006412

36. Akil, C., and Robinson, R. C. (2018) Genomes of Asgard archaea encode profilins that regulate actin. *Nature* **562**, 439–443

37. Kursula, I., Kursula, P., Ganter, M., Panjikar, S., Matuschewski, K., and Schuler, H. (2008) Structural basis for parasite-specific functions of the divergent profilin of *Plasmodium falciparum. Structure* **16**, 1638–1648

38. Dominguez, R. (2016) The WH2 domain and actin nucleation: necessary but insufficient. *Trends Biochem. Sci.* **41**, 478–490

39. Lu, J., and Pollard, T. D. (2001) Profilin binding to poly-L-proline and actin monomers along with ability to catalyze actin nucleotide exchange is required for viability of fission yeast. *Mol. Biol. Cell* **12**, 1161–1175

40. Colombo, J., Antkowiak, A., Kogan, K., Kotila, T., Elliott, J., Guillotin, A., *et al.* (2021) A functional family of fluorescent nucleotide analogues to investigate actin dynamics and energetics. *Nat. Commun.* **12**, 548

41. De La Cruz, E. M., and Pollard, T. D. (1995) Nucleotide-free actin: stabilization by sucrose and nucleotide binding kinetics. *Biochemistry* **34**, 5452–5461

42. Kasai, M., Nakano, E., and Oosawa, F. (1965) Polymerization of actin free from nucleotides and divalent cations. *Biochim. Biophys. Acta* **94**, 494–503

43. Petrella, E. C., Machesky, L. M., Kaiser, D. A., and Pollard, T. D. (1996) Structural requirements and thermodynamics of the interaction of proline peptides with profilin. *Biochemistry* **35**, 16535–16543

44. Otomo, T., Tomchick, D. R., Otomo, C., Panchal, S. C., Machius, M., and Rosen, M. K. (2005) Structural basis of actin filament nucleation and processive capping by a formin homology 2 domain. *Nature* **433**, 488–494

45. Schutt, C. E., Karlen, M., and Karlsson, R. (2022) A structural model of the profilin-formin pacemaker system for actin filament elongation. *Sci. Rep.* **12**, 20515

46. Sunter, J. D., Yanase, R., Wang, Z., Catta-Preta, C. M. C., Moreira-Leite, F., Myskova, J., *et al.* (2019) *Leishmania* flagellum attachment zone is critical for flagellar pocket shape, development in the sand fly, and pathogenicity in the host. *Proc. Natl. Acad. Sci. U. S. A.* **116**, 6351–6360

47. Survery, S., Hurtig, F., Haq, S. R., Eriksson, J., Guy, L., Rosengren, K. J., *et al.* (2021) Heimdallarchaea encodes profilin with eukaryotic-like actin regulation and polyproline binding. *Commun. Biol.* **4**, 1024

48. Bhargav, S. P., Vahokoski, J., Kallio, J. P., Torda, A. E., Kursula, P., and Kursula, I. (2015) Two independently folding units of *Plasmodium* profilin suggest evolution via gene fusion. *Cell Mol. Life Sci.* **72**, 4193–4203

49. Moreau, C. A., Quadt, K. A., Piirainen, H., Kumar, H., Bhargav, S. P., Strauss, L., *et al.* (2020) A function of profilin in force generation during malaria parasite motility that is independent of actin binding. *J. Cell Sci.* **134**, jcs.233775

50. Ignatev, A., Bhargav, S. P., Vahokoski, J., Kursula, P., and Kursula, I. (2012) The lasso segment is required for functional dimerization of the *Plasmodium* formin 1 FH2 domain. *PLoS One* **7**, e33586

51. Skillman, K. M., Daher, W., Ma, C. I., Soldati-Favre, D., and Sibley, L. D. (2012) *Toxoplasma gondii* profilin acts primarily to sequester G-actin while formins efficiently nucleate actin filament formation *in vitro*. *Biochemistry* **51**, 2486–2495

52. Kaksonen, M., and Roux, A. (2018) Mechanisms of clathrin-mediated endocytosis. *Nat. Rev. Mol. Cell Biol.* **19**, 313–326

53. Kaksonen, M., Toret, C. P., and Drubin, D. G. (2006) Harnessing actin dynamics for clathrin-mediated endocytosis. *Nat. Rev. Mol. Cell Biol.* **7**, 404–414

54. Gomez, T. S., and Billadeau, D. D. (2009) A FAM21-containing WASH complex regulates retromer-dependent sorting. *Dev. Cell* **17**, 699–711

55. Derivery, E., Sousa, C., Gautier, J. J., Lombard, B., Loew, D., and Gautreau, A. (2009) The Arp2/3 activator WASH controls the fission of endosomes through a large multiprotein complex. *Dev. Cell* **17**, 712–723

56. Linardopoulou, E. V., Parghi, S. S., Friedman, C., Osborn, G. E., Parkhurst, S. M., and Trask, B. J. (2007) Human subtelomeric WASH genes encode a new subclass of the WASP family. *PLoS Genet.* **3**, e237

57. Rotty, J. D., Wu, C., Haynes, E. M., Suarez, C., Winkelman, J. D., Johnson, H. E., *et al.* (2015) Profilin-1 serves as a gatekeeper for actin assembly by Arp2/3-dependent and -independent pathways. *Dev. Cell* **32**, 54–67

58. Suarez, C., Carroll, R. T., Burke, T. A., Christensen, J. R., Bestul, A. J., Sees, J. A., *et al.* (2015) Profilin regulates F-actin network homeostasis by favoring formin over Arp2/3 complex. *Dev. Cell* **32**, 43–53

59. Scholz, J., Besir, H., Strasser, C., and Suppmann, S. (2013) A new method to customize protein expression vectors for fast, efficient and background free parallel cloning. *BMC Biotechnol.* **13**, 12

60. Kotila, T., Wioland, H., Enkavi, G., Kogan, K., Vattulainen, I., Jegou, A., *et al.* (2019) Mechanism of synergistic actin filament pointed end depolymerization by cyclase-associated protein and cofilin. *Nat. Commun.* **10**, 5320

61. Spudich, J. A., and Watt, S. (1971) The regulation of rabbit skeletal muscle contraction. I. Biochemical studies of the interaction of the tropomyosin-troponin complex with actin and the proteolytic fragments of myosin. *J. Biol. Chem.* **246**, 4866–4871

62. Vonrhein, C., Flensburg, C., Keller, P., Sharff, A., Smart, O., Paciorek, W., *et al.* (2011) Data processing and analysis with the autoPROC toolbox. *Acta Crystallogr. D Biol. Crystallogr.* **67**, 293–302

63. Kabsch, W. (2010) Xds. *Acta Crystallogr. D Biol. Crystallogr.* **66**, 125–132

64. Evans, P. R., and Murshudov, G. N. (2013) How good are my data and what is the resolution? *Acta Crystallogr. D Biol. Crystallogr.* **69**, 1204–1214

ASBMB

65. Winn, M. D., Ballard, C. C., Cowtan, K. D., Dodson, E. J., Emsley, P., Evans, P. R., *et al.* (2011) Overview of the CCP4 suite and current developments. *Acta Crystallogr. D Biol. Crystallogr.* **67**, 235–242

66. Langer, G., Cohen, S. X., Lamzin, V. S., and Perrakis, A. (2008) Automated macromolecular model building for X-ray crystallography using ARP/wARP version 7. *Nat. Protoc.* **3**, 1171–1179

67. Murshudov, G. N., Skubak, P., Lebedev, A. A., Pannu, N. S., Steiner, R. A., Nicholls, R. A., *et al.* (2011) REFMAC5 for the refinement of macromolecular crystal structures. *Acta Crystallogr. D Biol. Crystallogr.* **67**, 355–367

68. Emsley, P., Lohkamp, B., Scott, W. G., and Cowtan, K. (2010) Features and development of Coot. *Acta Crystallogr. D Biol. Crystallogr.* **66**, 486–501

69. Liebschner, D., Afonine, P. V., Baker, M. L., Bunkoczi, G., Chen, V. B., Croll, T. I., *et al.* (2019) Macromolecular structure determination using X-rays, neutrons and electrons: recent developments in Phenix. *Acta Crystallogr. D Struct. Biol.* **75**, 861–877

70. Beneke, T., Madden, R., Makin, L., Valli, J., Sunter, J., and Gluenz, E. (2017) A CRISPR Cas9 high-throughput genome editing toolkit for kinetoplastids. *R. Soc. Open Sci.* **4**, 170095

71. Wheeler, R. J., Sunter, J. D., and Gull, K. (2016) Flagellar pocket restructuring through the *Leishmania* life cycle involves a discrete flagellum attachment zone. *J. Cell Sci.* **129**, 854–867

72. Holm, L. (2022) Dali server: structural unification of protein families. *Nucleic Acids Res.* **50**, W210–W215

73. Rebowski, G., Boczkowska, M., Drazic, A., Ree, R., Goris, M., Arnesen, T., *et al.* (2020) Mechanism of actin N-terminal acetylation. *Sci. Adv.* **6**, eaay8793

74. Gaucher, J. F., Mauge, C., Didry, D., Guichard, B., Renault, L., and Carlier, M. F. (2012) Interactions of isolated C-terminal fragments of neural Wiskott-Aldrich syndrome protein (N-WASP) with actin and Arp2/3 complex. *J. Biol. Chem.* **287**, 34646–34659

75. Hertzog, M., van Heijenoort, C., Didry, D., Gaudier, M., Coutant, J., Gigant, B., *et al.* (2004) The beta-thymosin/WH2 domain; structural basis for the switch from inhibition to promotion of actin assembly. *Cell* **117**, 611–623

76. Ferron, F., Rebowski, G., Lee, S. H., and Dominguez, R. (2007) Structural basis for the recruitment of profilin-actin complexes during filament elongation by Ena/VASP. *EMBO J.* **26**, 4597–4606

77. Paavilainen, V. O., Oksanen, E., Goldman, A., and Lappalainen, P. (2008) Structure of the actin-depolymerizing factor homology domain in complex with actin. *J. Cell Biol.* **182**, 51–59

78. Irobi, E., Aguda, A. H., Larsson, M., Guerin, C., Yin, H. L., Burtnick, L. D., *et al.* (2004) Structural basis of actin sequestration by thymosin-beta4: implications for WH2 proteins. *EMBO J.* **23**, 3599–3608